A 46-channel Vector Stimulator with 50mV Worst-Case Common-Mode Artifact for Low-Latency Adaptive Closed-Loop Neuromodulation

Arindam Mandal, Diego Peña, Rajesh Pamula†, Karam Khateeb, Logan Murphy, Azadeh Yazdan-Shahmorad, Steve Perlmutter, Forrest Pape‡, Jacques C. Rudell, Visvesh Sathe; University of Washington, †Skyworks, ‡Medtronic Inc.

Neural implants for closed-loop therapeutic neuromodulation – recording, processing, and delivering state and activity dependent neural stimulation to targeted regions of interest (ROIs) in the brain – are emerging as critical enablers of ground-breaking treatments of a wide range of neurological diseases and disorders. While existing systems [1-4] deliver electrical stimulation by placing electrodes in close proximity to target neurons, the capability for low-latency configurable stimulation that is spatially localized remains unrealized. Meanwhile, architectures that enable uninterrupted recording, maintain high voltage compliance and achieve excellent charge balance remain critical for implantable stimulators.

Vector current stimulation is an emerging technique for achieving ROI-targeted neural stimulation and involves simultaneous current stimulation across multiple electrodes [5]. However, any imbalance between the total source and sink currents (I_X) results in common mode (CM) artifacts – stimulation induced common mode voltage excursions at the recording sites – which can interrupt recording. Realizing arbitrary stimulus waveforms exacerbates imbalance which must be effectively compensated.

This paper presents a 46 channel 26V compliant adaptive stimulator designed for low-latency adaptive neuromodulation, implemented in a 180nm BCD process without a deep N-well, capable of delivering targeted electrical stimulation of up to 2mA/ch. (Fig. 1). This paper introduces 1) Computationally guided vector stimulation to target specific ROIs; 2) Integrated SRAM to enable low-latency selection and delivery of user-defined stimulation waveforms; 3) A circuit-architecture anchors the stimulation CM to the tissue to suppress CM artifacts; and 4) Effective run-time current imbalance compensation despite multi-electrode stimulation with arbitrary current waveforms. Applied together, techniques 3 and 4 enable worst-case CM artifacts to be suppressed to less than 50mV.

Fig. 2 outlines the proposed architecture for configurable stimulation and imbalance compensation. A Look-up Table (*LUT*), indexed by stimulation recipes, contains offset and stop entries to select a suitable address range for 46 memory banks – one for each stimulator channel. Each memory entry consists of a time-stamp, an I-DAC code, current polarity and a passive regeneration enable bit. Successive memory entries describe a stimulation waveform through a sequence of time-current pairs. Multiple stimulation traces can be stored in each bank - up to 96 entries. Stimulation recipes can thus be continuously selected and delivered with single cycle latency.

The output current delivered by each of the 46 current drivers is controlled by its *I-DAC* code with a programmable 5-20μA LSB. Inaccuracies resulting from gain and integral non-linearity errors across each of the 46 drivers are corrected through an offline calibration to minimize vector accuracy and suppress I_X to sub-LSB magnitude. To further suppress I_X and avoid prohibitive CM stimulation artifacts and electrode charge accumulation, we propose a combination of two techniques – concurrent and residual imbalance compensation, (CIC) and (RIC) respectively. CIC applies a trained, compensation current waveform through a dedicated channel using a higher-resolution DAC (1/8 of driver LSB) for continuous imbalance cancellation, suppressing the artifact to below 50mV under worst case conditions. Any residual electrode charge accumulation is corrected using RIC through a series of narrow correction pulses after a user-defined number of stimulation cycles. CIC and RIC waveform templates are unique to each part and recipe and are autonomously derived and stored for use during calibration.

Fig. 3 details the stimulation driver and passive regeneration switch design. Series *SRC* and *SINK* switches in the 5V digital domain control the driver current polarity. A wide-swing cascode current mirror maximizes driver compliance while providing adequate output impedance (> 4MΩ). The passive regeneration switch connects each driver output to the common V_{CM} node through the tissue interface, discharging any residual electrode charge. Bootstrapping is employed to allow the 5V-swing *REGEN* signal relative to the chip-ground (-14V) to control V_{CM}-source connected switches at 0V.

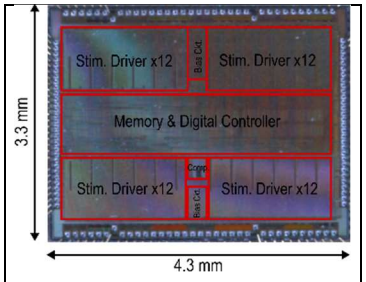

Die micrograph.

The ability of the proposed architecture to suppress CM artifacts is evaluated through experiments in a saline bath (Fig. 4) using a 200μA bipolar, biphasic stimulation with an arbitrarily chosen source and sink pair. Without a tissue/saline anchored V_{CM} connection, the imbalance between the source and sink currents generates a tissue /saline CM voltage (relative to V_{CM}) of up to 5V during stimulation, which can prevent uninterrupted recording. With an electrode anchoring the tissue/saline potential to V_{CM}, the CM excursion is limited by $I_X Z_E$ – approximately 0.13V for this experiment. CIC and RIC further reduce this imbalance induced CM artifact to less than 50mV.

Areas activated by vector stimulation are contrasted with those of differential stimulation [1] in Fig. 5. The current vector used to target the ROIs is obtained by first establishing a current basis made up of 75 independent dipole current combinations of source-sink channel pairs (IBi) to enforce current balance (I_X=0). Next, a channel matrix (***H***) of the saline bath was built using a discrete space electrical model with sufficient resolution. ***H*** is populated with the second spatial derivative (*D2*) of the voltage in the direction of axons (arbitrarily assigned to be the x-axis for this experiment) at each location resulting from unit current flow for each basis. Finally, a convex optimization problem was formulated using ***H*** in a manner similar to [5], to maximize *D2* in each ROI under the constraint of maintaining *D2* to be below a specified excitation threshold elsewhere. The solution of this problem delivers the vector current that delivers stimulation with superior ROI localization compared to differential stimulation. Because continuous *D2* measurement across the array is not feasible, we present the simulated regions of excitation, cross-validated with measurements at the electrode pitch. A good level of correlation was found between simulations and measurements, indicated by an R^2 correlation score of 0.994.

The designed stimulator is interfaced to implanted electrodes in the cervical spinal cord of a sedated rat for *in-vivo* measurements (Fig. 6). Biphasic, 210μA amplitude, 200μs wide stimulus pulses are applied at a 0.5Hz frequency, and motor evoked potentials are recorded in the ipsilateral triceps muscle using an Intan RHD2000 chip demonstrate the suitability of the implemented stimulator for *in-vivo* experiments.

This paper demonstrates the effectiveness of vector stimulation and integrated memory in enabling targeted, low-latency closed-loop adaptive neuromodulation. Concurrent stimulation of a large number of electrodes improves localization but exacerbates current imbalance, placing renewed emphasis on techniques to mitigate both current imbalance and their associated CM artifacts.

Acknowledgement: This project was funded in part by an NSF CAREER grant and by Medtronic Inc. We thank Mentor Graphics for use of the AFS simulation engine.

References:

[1] D. Rozgić *et al*., "A 0.338 cm^3, Artifact-Free, 64-Contact Neuromodulation Platform for Simultaneous Stimulation and Sensing" TBioCAS, Feb. 2019

[2] B. C. Johnson *et al*., "An implantable 700μW 64-channel neuromodulation IC for simultaneous recording and stimulation with rapid artifact recovery," VLSI, 2017

[3] H. Kassiri *et al*., "Rail-to-Rail-Input Dual-Radio 64-Channel Closed-Loop Neurostimulator," JSSC, Nov. 2017

[4] E. Greenwald *et al*., "A CMOS Current Steering Neurostimulation Array With Integrated DAC Calibration and Charge Balancing," TBioCAS, April 2017

[5] D. Anderson et. al., "Optimized programming algorithm for cylindrical and directional deep brain stimulation electrodes," *JNE, Jan.* 2018

2021 IEEE Custom Integrated Circuits Conference (CICC) | 978-1-7281-7581-2/20/$31.00 ©2021 IEEE | DOI: 10.1109/CICC51472.2021.9431493

978-1-7281-7581-2/21/$31.00 ©2021 IEEE

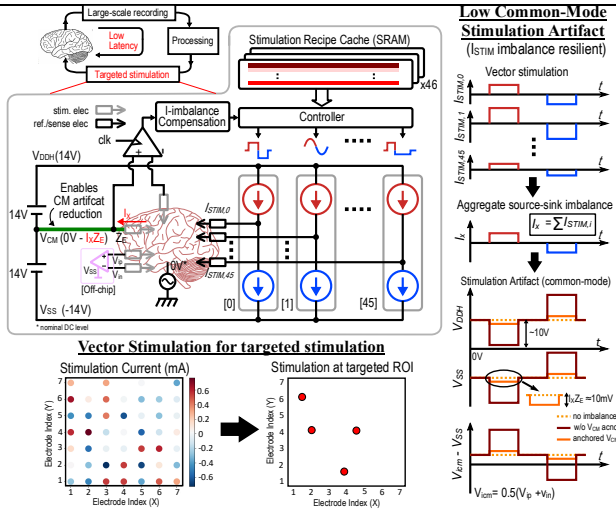

Fig. 1. (Top left) Demonstration of low-latency targeted neural stimulation. (Bottom left) Vector stimulation enables current steering to activate ROIs in the brain. (Right) Anchoring the V_{CM} to the tissue provides <50mV CM artifact at a recording interface referred to V_{SS}

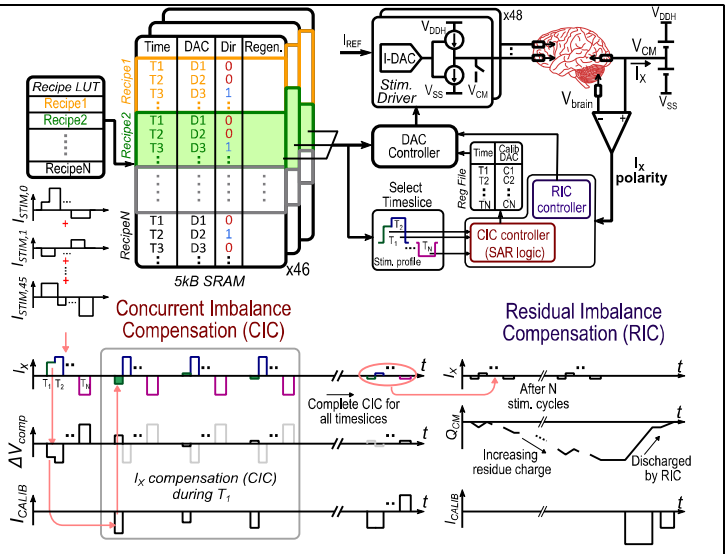

Fig. 2. (Top) Chip architecture. (Bottom left) CIC corrects for the imbalance current in each timeslice. (Bottom right) RIC to discharge any accumulated charge on the tissue/saline anchor electrode.

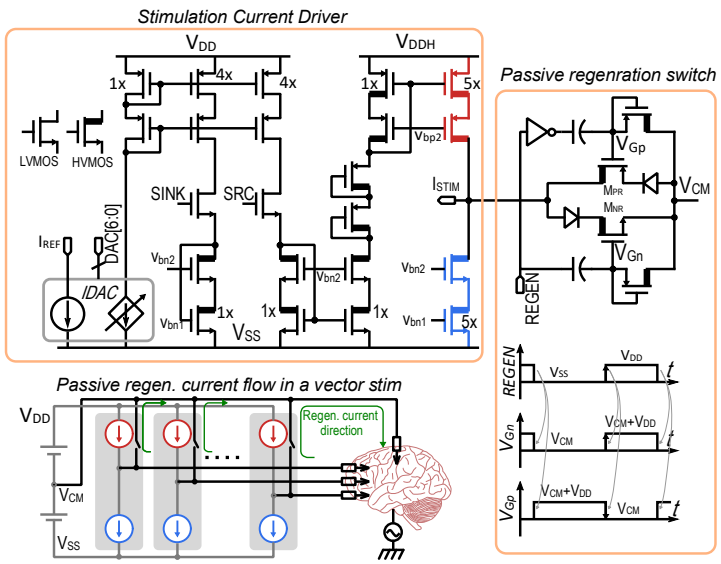

Fig. 3. Current driver schematic with passive regeneration switch

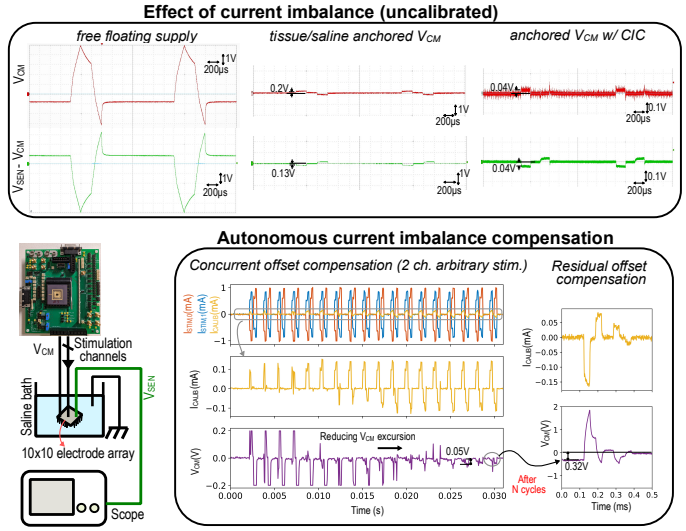

Fig. 4. (Left) Test setup for saline measurements. (Top right) Impact of current imbalance at V_{CM} and at a recording channel referred to V_{CM}. (Bottom right) CIC, RIC applied to lower the V_{CM} excursion

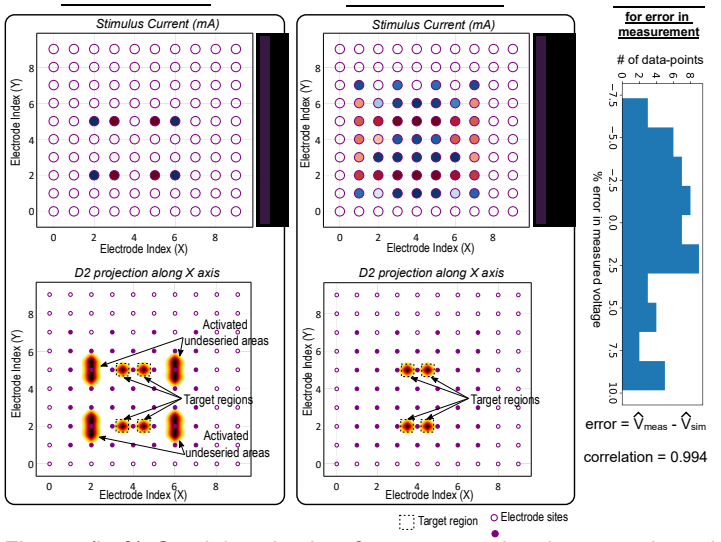

Fig. 5. (Left) Spatial activation for a conventional approach and proposed method. Axons in ROI are assumed to oriented along the X axis. (Right) Error in saline measurement.

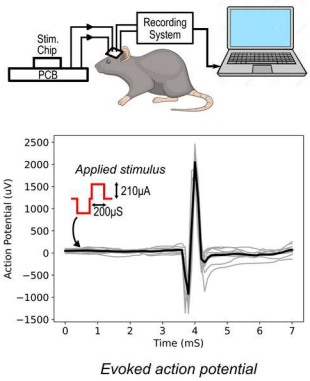

	TBioCAS 2019 [1]	VLSI 2017 [2]	JSSC 2017 [3]	TBioCAS 2017 [4]	This work
Technology	HV 180nm	HV 180nm	130nm	180nm	HV 180nm
Stim. drivers	8	4	64	8	46
Compliance	9V	12V	3.1V	3V	26V
Max. current	5.1mA	5.04mA	1.35mA	0.25mA	2mA
DAC res.	7bit	8bit	8bit	8bit	7 bit
Area/ch(mm²)	0.79 *	0.11 *	0.0016 *	0.064	0.12
Stim. method	Bipolar	Bipolar	Bipolar	Tripolar	Vector
Waveform	Arbitrary	Arbitrary	Arbitrary	Biphasic	Arbitrary
Stim. reconfig	No	Yes(4ms)	No	No	Yes
Targeted stim	No	No	No	No	Yes
V_{CM} excursion	N.R.	N.R.	N.R.	N.R.	< 50mV

* Estimated from die-photo

Fig. 6. (Top) Test setup for in-vivo stimulation and record. (Bottom). Overlayed (gray) and average (black) motor evoked potentials in triceps muscle in response to stimulation in the cervical spinal cord. (Right) Comparison table